

<https://doi.org/10.1038/s42003-025-08132-6>

Brain connectome gradient dysfunction in patients with end-stage renal disease and its association with clinical phenotype and cognitive deficits

Check for updates

Peng Li^{1,2,3,6}, Nan Li^{4,6}, Li Ren⁵, Yan-Ping Yang⁵, Xin-Yi Zhu³, Hui-Jie Yuan³, Zhao-Yao Luo³, Jun-Ya Mu^{3,7} ✉, Wen Wang^{1,7} ✉ & Ming Zhang³ ✉

A cortical hierarchical architecture is vital for encoding and integrating sensorimotor-to-cognitive information. However, whether this gradient structure is disrupted in end-stage renal disease (ESRD) patients and how this disruption provides valuable information for potential clinical symptoms remain unknown. We prospectively enrolled 77 ESRD patients and 48 healthy controls. Using resting-state functional magnetic resonance imaging, we studied ESRD-related hierarchical alterations. The Neurosynth platform and machine-learning models with 10-fold cross-validation were applied. ESRD patients had abnormal gradient metrics in core regions of the default mode network, sensorimotor network, and frontoparietal network. These changes correlated with creatinine, depression, and cognitive functions. A logistic regression classifier achieved a maximum performance of 84.8% accuracy and 0.901 area under the ROC curve (AUC). Our results highlight hierarchical imbalances in ESRD patients that correlate with diverse cognitive deficits, which may be used as potential neuroimaging markers for clinical symptoms.

End-stage renal disease (ESRD), the most severe stage of chronic kidney disease, is defined as an estimated glomerular filtration rate less than 15 mL/min/1.73 m². As a growing global public health problem¹, ESRD patients are at a significantly higher risk of developing brain dysfunction, such as cognitive impairment², sensorimotor abnormalities³, and mood disorders⁴, than the general population. In addition to the characteristic clinical symptoms of uremia^{3,5,6}, including uremia pruritus, frailty, anxiety, depression, and fatigue, neuropsychological studies reveal that ESRD patients demonstrate deficits in low-level sensory processing^{7,8} (e.g., pain perception, sensorimotor processing) and higher-order cognitive functions^{2,9} (e.g., learning, attention, memory, decision making, and reasoning). Our previous studies have revealed widespread brain structure and function abnormalities in ESRD patients^{10–13}, but the neural mechanisms underlying these diverse sensory-cognitive deficits remain largely unknown.

Resting-state functional MRI (R-fMRI) has been established as an important neuroimaging tool for identifying the neuropathological mechanisms underlying sensorimotor abnormalities and higher-order cognitive impairment in ESRD patients by analyzing blood oxygen level dependent (BOLD) signals^{12–17}. These neuroimaging studies mainly focused on aberrant functional connectivity in the core regions of the default mode network (DMN), such as the medial prefrontal cortex (mPFC) and precuneus^{12,14}, decreased functional connectivity in core regions of the sensorimotor network¹⁵, abnormal interactions between the cognitive control network and affective network¹⁶, and complex relationships between DMN isolation, gut microbiota, and systemic inflammation¹⁷. However, previous network results were analyzed based on separate analytical frameworks, i.e., they all involved networks processed at similar levels, which hardly reflected the hierarchical characteristics of brain macroscale organization in ESRD patients.

¹Department of Radiology & Functional and Molecular Imaging Key Lab of Shaanxi Province, The Second Affiliated Hospital of Air Force Medical University, Xi'an, Shaanxi, China. ²Department of Medical Imaging, Nuclear Industry 215 Hospital of Shaanxi Province, Xianyang, Shaanxi, China. ³Department of Medical Imaging, First Affiliated Hospital of Xi'an Jiaotong University, Xi'an, Shaanxi, China. ⁴Department of Medical Laboratory, Xidan Group Hospital, Xi'an, Shaanxi, China. ⁵Department of Nephrology, Nuclear Industry 215 Hospital of Shaanxi Province, Xianyang, Shaanxi, China. ⁶These authors contributed equally: Peng Li, Nan Li. ⁷These authors jointly supervised this work: Jun-Ya Mu, Wen Wang, Ming Zhang. ✉e-mail: junyamu@xjtu.edu.cn; wangwen@fmmu.edu.cn; zhangming01@mail.xjtu.edu.cn

A cortical hierarchical architecture is one of the basic organizing principles of the human brain, which enables the process of encoding and integrating information from sensation to cognition¹⁸. Recent advances in conceptual and methodological studies have revealed that macroscale brain organization and hierarchical features are reflected in a compact manner using multivariate machine learning approaches that map to low-dimensional manifold representations, described as cortical gradients^{19,20}. Researchers can use the gradient decomposition framework of R-fMRI to decompose the functional brain network into different gradient components and present relative differences in connectivity patterns among regions along a continuous spectrum to capture the topological properties of the connectomes^{19,21}. The first principal gradient describes a continuous transition of neural function that anchors unimodal primary sensorimotor areas and high-order transmodal DMN regions at two opposite ends of a spectrum²². Additionally, the second principal gradient separates the somatomotor and auditory cortex from the visual cortex, whereas the third principal gradient represents the hierarchical cortical axes of multiple demand-rest patterns^{19,23}. The principal gradients have been widely revealed to characterize hierarchical cognition processes of language, working memory, and attention^{24,25}, as well as perturbations in various mental and neuropsychiatric disorders such as major depressive disorder²⁶, autism²⁷, schizophrenia^{28,29}, and epilepsy³⁰. Previous studies have demonstrated aberrant intrinsic brain activity and functional connectivity that involves the primary sensorimotor regions and transmodal DMN in ESRD patients, which are related to sensory-cognitive deficits and clinical risk factors (e.g., uremic toxin accumulation^{12,14}, anemia¹⁶, systemic inflammation¹⁷, calcium and phosphorus metabolism disorders^{15,16}). However, no research has yet revealed whether and how the functional connectome gradients are disrupted in these patients, or whether such disruptions could serve as potential biomarkers for clinical symptoms.

To address these gaps, we collected various clinical and R-fMRI data from 77 ESRD patients and 48 healthy controls (HC). The Neurosynth (<https://neurosynth.org/>) platform³¹ was used to investigate the association between ESRD-related functional gradient alterations and meta-analytic cognitive terms. Furthermore, multiple machine learning classification models were utilized to investigate the discriminative power of connectome gradient features derived from ESRD patients and controls. Specifically, we hypothesized that (i) the principal gradients are disrupted in ESRD patients in terms of both global and focal connectome gradient metrics of primary

sensorimotor and transmodal systems; (ii) the regions with alterations of connectome gradient are associated with multiple functional domains and ESRD-related clinical risk factors involving uremic toxin accumulation, calcium and phosphorus metabolism disorders, systemic inflammation, and mood disorder. Our findings demonstrated that the dysfunctional regions within these core connectome gradients functioned as neurological biomarkers for ESRD. This highlights their significance in elucidating the large-scale brain organization as well as the hierarchical characteristics that underpin ESRD and its associated cognitive phenotype.

Results

Demographic, clinical, and neuropsychological results

Figure 1 shows the entire process of patients with ESRD from screening to inclusion. Table 1 shows demographic and clinical data for each group. No significant between-group differences in age, sex, or educational level were observed. ESRD patients demonstrated poorer performances in subitems of auditory verbal learning test-Huashan version (AVLT-H) (immediate recall [$P < 0.001$], long-term recall [$P < 0.001$], and recognition [$P = 0.004$]) and subitems of MoCA (total score [$P < 0.001$], visuospatial [$P < 0.001$], name [$P = 0.032$], language [$P < 0.001$], abstraction [$P < 0.001$], and delayed memory [$P < 0.001$]) compared with the HC group in terms of neuropsychological tests. Furthermore, ESRD patients exhibited poorer performances in TMT ($P < 0.001$), BAI ($P < 0.001$), and BDI ($P < 0.001$) compared with the HC group.

Alterations in the connectome gradients in ESRD patients

We primarily focused on ESRD-related alterations in the first three components, which explained 38% of the variance. The first principal gradient explained $15.6\% \pm 1.9\%$ of the total connectivity variance (ESRD, $15.7\% \pm 2.0\%$; HC, $15.5\% \pm 1.7\%$), which showed a gradual axis from the low-level primary visual/sensorimotor networks (VIS/SMN) to the transmodal DMN, with intermediary networks in between (Fig. 2a), replicating the recent functional connectome gradient data in healthy adults¹⁹. Gradient 2 explained $12.5\% \pm 1.5\%$ of the total connectivity variance (ESRD, $12.4\% \pm 1.4\%$; HC, $12.8\% \pm 1.5\%$), which extended between the SMN and the VIS (Fig. 2b). Gradient 3 explained $10.2\% \pm 1.0\%$ of the total connectivity variance (ESRD, $10.0\% \pm 0.9\%$; HC, $10.4\% \pm 1.0\%$), which extended between the SMN and the VIS (Fig. 2c). The between-group statistical comparisons of global gradient

Fig. 1 | Flowchart demonstrating the phases in patients with end-stage renal disease from screening to inclusion and completion of the study.

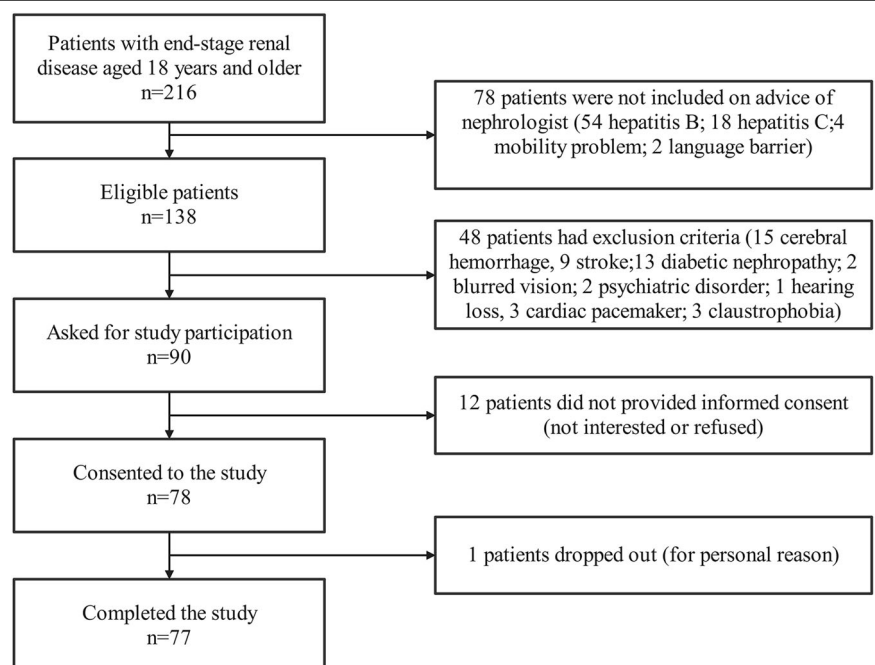


Table 1 | Demographic, clinical characteristics, and neuropsychological assessment in ESRD patients and HC

Variable	HC (n = 48)	ESRD (n = 77)	t value	P value
Age (years)	31.47 (8.16)	34.83 (10.05)	1.945	0.054 ^b
Gender (M/F)	23 (25)	50 (27)	3.525 ^a	0.065 ^a
Education (years)	11.94 (1.86)	11.21 (2.33)	-1.834	0.069 ^b
Dialysis vintage (months)	/	38.74 (29.61)	/	/
Creatinine (μmol/L)	/	912.68 (219.84)	/	/
Urea (mmol/L)	/	23.67 (7.26)	/	/
Kt/V	/	1.46 (0.18)	/	/
Hemoglobin (g/L)	/	107.61 (19.02)	/	/
Hematocrit (%)	/	32.93 (5.58)	/	/
Cystatin C (μg/mL)	/	6.15 (3.20)	/	/
Potassium (mmol/L)	/	4.82 (0.72)	/	/
Sodium (mmol/L)	/	142.35 (3.28)	/	/
Phosphorus (mmol/L)	/	1.77 (0.54)	/	/
Calcium (mmol/L)	/	2.13 (0.34)	/	/
Parathormone (ng/L)	/	632.87 (450.50)	/	/
Medication	N	%		
AT1-blocker	67	87	/	/
Beta-blocker	55	71	/	/
EPO	74	96	/	/
Antidepressants	0	0	/	/
Antihistamines	0	0	/	/
Analgesics	0	0	/	/
Vitamin D	47	61	/	/
Calcium antagonists	10	13	/	/
AVLT-H				
IR-S	27.76 (3.70)	25.17 (4.45)	4.71	<0.001 ^{b,c}
SR-S	10.25 (1.21)	9.58 (1.65)	0.93	0.013 ^{b,c}
LR-S	10.19 (1.28)	9.00 (1.73)	2.17	<0.001 ^{b,c}
REC-S	11.81 (0.50)	11.36 (1.00)	2.26	0.004 ^{b,c}
MoCA				
Total score	27.42 (2.24)	23.87 (2.85)	5.06	<0.001 ^{b,c}
Visuospatial	4 (1)	4 (2)	0.70	<0.001 ^{c,d}
Name	3 (0)	3 (0)	2.24	0.032 ^{c,d}
Attention	6 (1)	6 (1)	0.26	0.085 ^d
Language	3 (1)	2 (0)	2.95	<0.001 ^{c,d}
Abstraction	2 (0)	1 (1)	5.56	<0.001 ^{c,d}
Orientation	6 (0)	6 (1)	-0.57	0.197 ^d
Delayed memory	5 (1)	4 (1)	2.67	<0.001 ^{c,d}
TMT	42.48 (13.33)	60.23 (28.38)	-4.75	<0.001 ^{b,c}
BDI	8.23 (5.22)	16.12 (10.46)	-3.35	<0.001 ^{b,c}
BAI	25.37 (2.76)	28.74 (6.03)	-3.16	<0.001 ^{b,c}

Table 1 (continued) | Demographic, clinical characteristics, and neuropsychological assessment in ESRD patients and HC

Variable	HC (n = 48)	ESRD (n = 77)	t value	P value
<p>ESRD end-stage renal disease, HC health controls, AVLT-H auditory verbal learning test-Huashan version, IR-S immediate recall score, SR-S short-term recall score, LR-S long-term recall score, REC-S recognition score, MoCA Montreal cognitive assessment, TMT trail-making test, BAI Beck anxiety inventory, BDI Beck depression inventory.</p> <p>^aAnalyzed with the chi-square test.</p> <p>^bAnalyzed with the independent two-sample t-test; data in parentheses have a 95% confidence interval, data are mean (standard deviation).</p> <p>^cIndicates a statistically significant difference after controlling for age, sex, and education level.</p>				
<p>metrics revealed that the primary-to-transmodal gradient (gradient 1) in ESRD patients demonstrated less spatial variation than that in HC [$P < 0.05$, false discovery rate (FDR) corrected, Fig. 3a].</p> <p>The between-group comparison of gradient 1 revealed decreases in ESRD patients mainly located in the transmodal mPFC, dorsal prefrontal cortex (dPFC), inferior parietal lobule (IPL), precuneus/posterior cingulate cortex (pCun/PCC), and middle temporal gyrus, together with increases mainly located in the somatomotor and visual cortices (Fig. 2a and Supplementary Table 1). A global histogram of gradient 1 revealed contracted extremes in ESRD patients relative to the HC range, whereas those in the middle axis increased (Fig. 2d). At the system level, ESRD patients demonstrated lower gradient scores in the DMN and frontoparietal network (FPCN) but higher scores in the SMN and VIS than the HC group (FDR corrected, Fig. 2g, j, Supplementary Table 4).</p> <p>The between-group comparison of gradient 2 revealed decreases in ESRD patients located in the mPFC and dorsolateral prefrontal cortex, together with increases mainly located in the somatomotor cortex and insula (Ins) (Fig. 2b and Supplementary Table 2). The histogram of gradient 2 revealed contracted extremes in ESRD patients relative to the HC range, whereas those in the middle axis decreased (Fig. 2e). At the system level, ESRD patients demonstrated lower gradient scores in the FPCN but higher scores mainly in the SMN, the ventral attention network (VAN), and VIS than the HC group (FDR corrected, Fig. 2h, k, Supplementary Table 4).</p> <p>The between-group comparison of gradient 3 revealed decreases in ESRD patients located in the mPFC, dPFC, and somatomotor cortex, together with increases mainly located in the posterior-medial frontal cortex (mpPFC), ventrolateral prefrontal cortex (vlPFC), and orbitofrontal cortex (Fig. 2c and Supplementary Table 3). The histogram of gradient 3 revealed contracted extremes in ESRD patients relative to the HC range, whereas those in the middle axis increased (Fig. 2f). At the system level, ESRD patients demonstrated lower gradient scores in the DMN and SMN but higher scores in the FPCN than the HC group (FDR corrected, Fig. 2i, l, Supplementary Table 4).</p>				
<p>Clinical and neuropsychological variables associated with gradient alterations in ESRD patients</p> <p>The correlation analysis of between-group gradient differences and clinical characteristics indicated a positive association between the somatomotor cortex of gradient 2 and serum creatinine levels in ESRD patients (Pearson correlation: $r = 0.464$, $P = 0.002$). The correlation analysis of between-group gradient differences and neuropsychological scores showed that the dPFC of gradient 2 was negatively correlated with BDI scores in ESRD patients (Pearson correlation: $r = -0.388$, $P = 0.045$), while Ins of gradient 1 was positively correlated with subitem of MoCA (name) scores of ESRD patients (Spearman correlation: $r = 0.419$, $P = 0.013$) (Fig. 3b).</p>				
<p>Meta-analytic cognitive functions related to gradient alterations in ESRD patients</p> <p>Figure 3c and Supplementary Tables 5–7 showed the results of meta-analytic cognitive terms. The regions with higher scores of gradient 1 in ESRD patients were correlated with several meta-analytic cognitive terms mainly involved in motor and sensory processes such as motor,</p>				

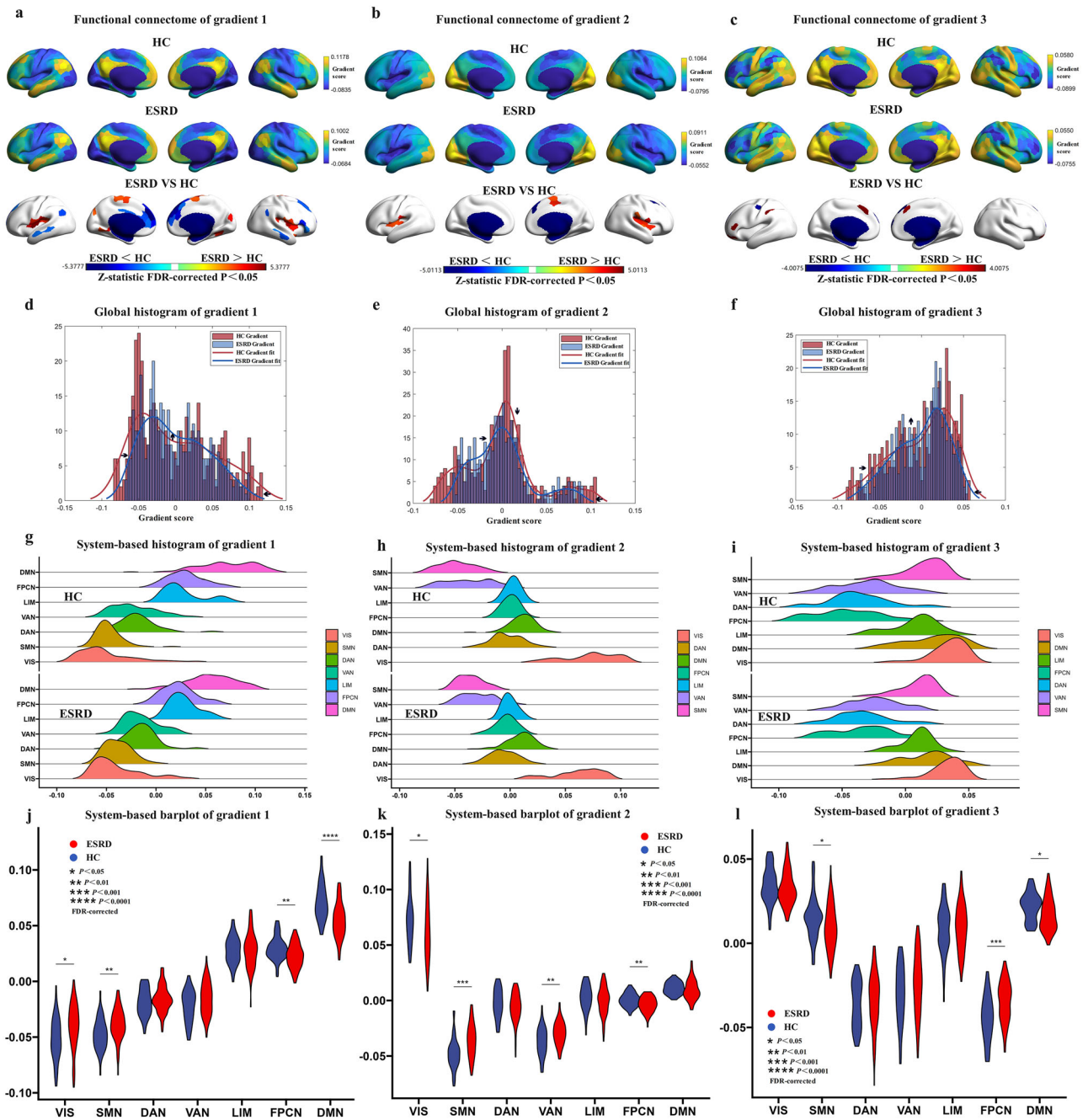


Fig. 2 | Connectome gradient mapping in ESRD patients and HC. **a** Gradient 1 was organized along a gradual axis from VIS/SMN to DMN. **b, c** Gradient 2 and gradient 3 extended between the SMN and the VIS. **a–c** Regions with similar connectivity patterns demonstrate similar coloring. The gradients were overall similar between-group, while lower/higher values in ESRD patients are presented as blue/red. The statistical significance level was set as P values of < 0.05 after FDR correction. **d–f** Global histograms of the gradients 1–3 showing contracted extremes in

ESRD patients relative to the HC range, whereas those of gradient 1 and gradient 3 in the middle axis increased and gradient 2 in the midrange decreased. **g–i.** System-based analysis of the gradient score between-group. VIS visual network, SMN sensorimotor network, DAN dorsal attention network, VAN ventral attention network, LIM limbic network, FPCN frontoparietal network, DMN default mode network.

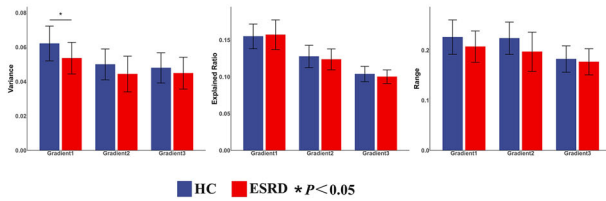
somatosensory, and sensorimotor processes. The regions with lower gradient 1 scores in ESRD patients were correlated with several high-order cognitive terms, including semantic, comprehension, language, and mind. The regions with higher scores of gradient 2 in ESRD patients were correlated with motor, movement, somatosensory, executive, vocal, and sensory processes. The regions with lower gradient 2 scores in ESRD patients were correlated with several high-order cognitive terms, including reward, choice, autonomic process, and decision making. Regions with higher scores of gradient 3 in ESRD patients were correlated with high-order cognitive

terms, including cognitive control, response inhibition, and conflict processes, whereas regions with lower scores of gradient 3 were correlated with guide and internally oriented cognitive processes.

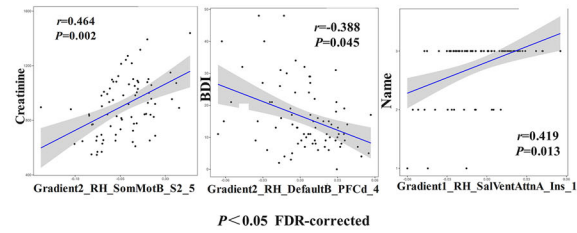
Feature selection and classification based on ESRD-related gradient alterations

After the dimension reduction using the least absolute shrinkage and selection operator (LASSO) method (Supplementary Fig. 2), 93 feature metrics from between-group differences of the gradient scores were reduced

a Global-level gradient metrics differences



b Functional gradients differences association with clinical and cognitive variables



c Cognitive terms of between-group gradient differences



Fig. 3 | Statistical comparison of gradient metrics. a Between-group differences in global metrics of the first three gradients. **b** Between-group differences in gradient scores and correlations with clinical and cognitive variables across all patients. **c** Word clouds of cognitive functions associated with brain regions showing lower

(blue) or higher (red) between-group gradient scores. The resulting font size of the cognitive term corresponds to the correlation coefficient (r) of the between-group Z-map of the first three gradients and the meta-analytic map of that word generated by Neurosynth. All correlations were significant ($P < 0.05$, FDR corrected).

to 10 features as input into seven classifiers to develop the corresponding classification models (Supplementary Fig. 3). These regions include: the right dPFC, right mpPFC, and left visual cortex in gradient 1, the right somatomotor cortex and left insula in gradient 2, and the right dPFC, the vPFC, and bilateral vlPFC in gradient 3. Finally, we used the 10-fold cross-validation to obtain the accuracy, sensitivity, specificity, and area under the curve (AUC) of the seven models. Among them, the accuracy and AUC of logistic regression were 84.8% and 0.901, respectively, which was better than those of the other classifier algorithms (Fig. 4a, Supplementary Tables 8 and 9). Figure 4b reveals the feature correlation heatmap. Supplementary Fig. 3 revealed that the top three contributing features were the right sensorimotor cortex of gradient 2, the right dPFC of gradient 3, and the left visual cortex of gradient 1.

Validation analyses

The results of validation analyses supported the robustness of our findings. Firstly, with respect to the between-group functional gradient metrics (the global, system, and regional levels) obtained under the temporal filtering with the ranges of 0.008–0.09 Hz demonstrated a high degree of similarity to those derived from the ranges of 0.01–0.08 Hz (Supplementary Fig. 1 and Supplementary Tables 10–13). Secondly, the results of the leave-one-out cross-validation (LOOCV) method were in general concordance with those obtained from the 10-fold cross-validation approach (Supplementary

Figs. 4–6 and Supplementary Tables 14 and 15). Finally, no significant differences in the mean framewise displacement (FD) values between-group (Supplementary Fig. 7).

Discussion

This is the first study to reveal connectome gradient dysfunction in ESRD patients and its association with clinical phenotype and cognitive deficits. Whether at the global, system, or regional levels, we revealed gradient metric abnormalities in core regions of the DMN, SMN, and FPCN in ESRD patients, which were associated with multiple functional domains. Serum creatinine accumulation and cognitive impairment might be associated with the disruption of the SMN and DMN in ESRD patients. Machine learning classification results revealed that gradient features of the core regions in the DMN and SMN can be used to discriminate ESRD patients from HC. Our results emphasized the imbalances in the functional connectome hierarchy in ESRD patients, which might be used as potential neuroimaging markers for clinical symptoms.

Network hierarchy has been widely known as a key principle of human brain organization, and gradients are thought to guide the direction of information flow through the cerebral cortex, making sensory signals increasingly associated with other information and being translated into more abstract cognitive representations^{20,22}. Our principal connectome gradient mapping revealed that both groups demonstrated a gradual axis

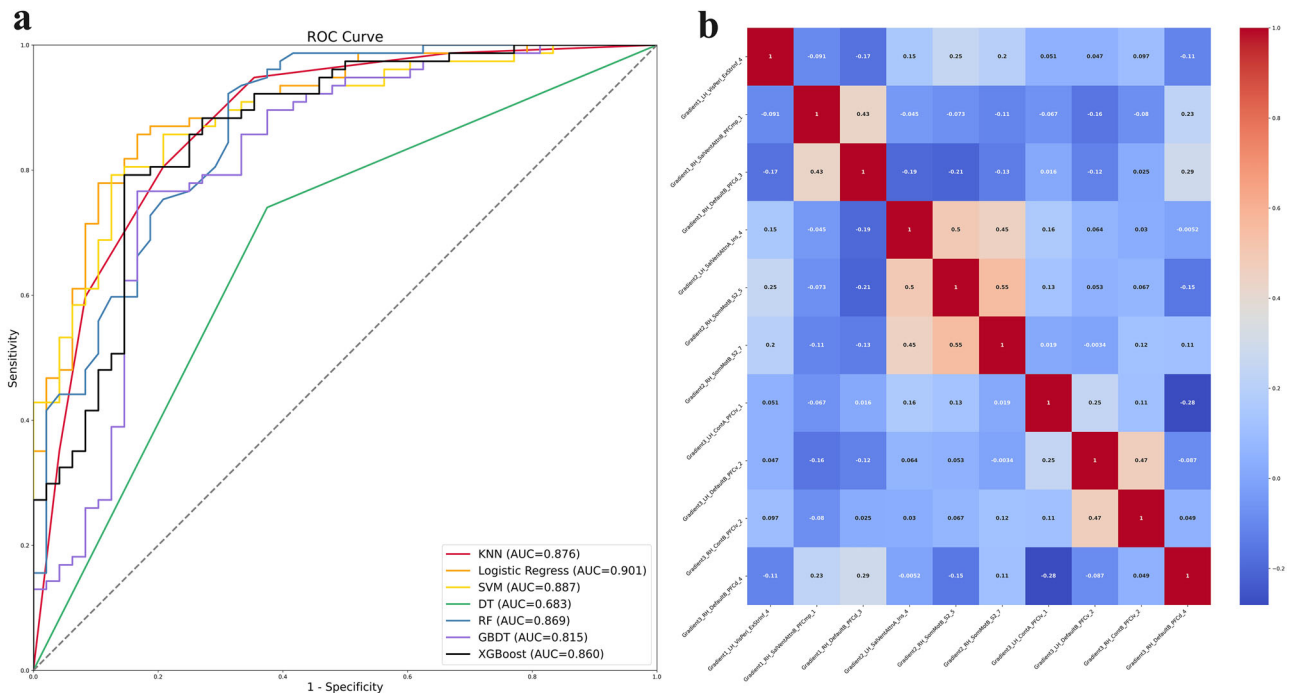


Fig. 4 | Performance of machine learning algorithms for classification. **a** ROC curve of the classifiers. The accuracy and AUC of logistic regression were 84.8% and 0.901, respectively, which was better than those of the other classifier algorithms.

b Features correlation heatmap. ROC receiver operating characteristic, AUC area under the curve, KNN k-nearest neighbor, SVM support vector machine, DT decision tree, RF random forest, GBDT gradient boosting decision tree.

from the low-level VIS and SMN to the transmodal DMN with intermediary networks in between. However, the smaller variance, contracted extremes, and increased midrange of the principal gradient represent a less differentiated connectivity pattern between the primary sensorimotor and transmodal DMN areas in ESRD patients. ESRD patients demonstrated lower gradient scores in the DMN but higher scores in the SMN and FPCN than the controls at the system level. Previous neuroimaging studies have revealed abnormal spontaneous neural activity and functional connectivity in the DMN hubs^{12,14,17}, such as mPFC, pCun/PCC, and IPL, associated with cognitive deficits in ESRD patients. Some sensorimotor symptoms in ESRD patients, such as restless leg syndrome, have recently been thought to be associated with abnormal functional connectivity in SMN¹⁵. The present results revealed a diminished segregation in ESRD patients between sensorimotor and executive control regions such as mpPFC, on the one hand, and transmodal hubs such as mPFC, IPL, and pCun/PCC on the other hand. The DMN is at a maximal geodesic distance from visual and sensorimotor systems in both anatomical space and functional connectivity¹⁹, indicating that neural activity in the DMN regions is probably comparably insulated from direct environmental input³². The maximum spatial separation and differentiation in the physical distance and connectivity dissimilarity guarantee the complete processing route from mapping concrete stimuli to integrating abstract concepts³³, while increasing the difference between primary and transmodal areas, avoiding interference from input noise, and facilitating abstract cognitive formation³⁴. Altogether, this study provided integrative evidence that cortical hierarchy organization dysfunction underlies system-level pathological interactions of sensorimotor and cognitive functions in ESRD patients.

One fundamental role of human neuroimaging is brain “decoding,” inferring a person’s cognitive state from their observed brain activity. Our previous neuroimaging studies have found that cognitive impairment in patients with ESRD were associated with decreased neural activity^{16,35}, demyelination¹³, abnormal cerebral perfusion¹¹, and neurovascular decoupling¹⁰, which were closely related to creatinine, urea, and hemodialysis adequacy. In this study, we focused on large-scale functional gradient abnormalities in patients with ESRD, and further explored the correlation

between such gradient abnormalities and clinical indicators and cognitive scales. Our results indicated that subterm of MoCA (name scores) were significantly positively correlated with the gradient value of the insula, while depression scores were significantly negatively correlated with the gradient value of the dPFC. These results suggest the basis of large-scale functional hierarchy structure of cognitive impairment and mood disorders in ESRD patients. In addition, by using the “decoder” function in the Neurosynth framework³¹, our meta-analytic cognitive results confirm that ESRD-related connectome gradient dysfunction were located in brain regions that involve multidomain cognitive functions, including lower-order sensorimotor processes and higher-order functions. The brain areas with lower functional gradient scores in ESRD patients were associated with higher-order cognitive functions, such as comprehension, language, reward, and executive function, whereas the areas with higher functional gradient scores were associated with sensorimotor functions, such as motor, somatosensory, and sensorimotor processes. ESRD patients frequently have motor control, sensory disorders, and higher-order cognitive deficits^{2,36,37}. Therefore, our results provide macroscale connectome gradient evidence for the underlying neural mechanisms of lower-order sensorimotor and higher-order cognitive impairment in ESRD patients.

The underlying brain injury mechanism of cognitive impairment in ESRD patients remains unclear, and one of the most important factors is the damage of brain structure and function caused by the disruption of the blood-brain barrier by urotoxic neurotoxins (such as creatinine, etc.)³. Patients with ESRD are associated with diverse sensorimotor disorders, such as restless leg syndrome and uremic pruritus, which were related to uremic toxin accumulation such as creatinine caused by inadequate dialysis treatment^{38,39}. As a small molecule water-soluble uremic toxin⁴⁰, serum creatinine level in ESRD patients was significantly positively correlated with gradient scores of the sensorimotor regions, indicating the role of uremic toxin in ESRD-related connectome gradient dysfunction. Although we did not evaluate the symptoms of uremic restless legs and uremic pruritus in ESRD patients, the results of meta-analytic cognitive terms also found that higher gradient values of the sensorimotor network was closely related to sensorimotor symptoms. Our previous neuroimaging studies have found

that hemodialysis adequacy index (Kt/V) and uremic toxins (creatinine and urea accumulation) were associated with cognitive impairment and cerebral neurovascular decoupling in ESRD patients¹⁰, while a single hemodialysis treatment significantly reduce the circulation of uremic toxins such as creatinine, thereby improving cognitive function and neurovascular coupling¹¹. Therefore, the results of this study found that the accumulation of creatinine in the blood circulation of ESRD patients is closely related to the gradient dysfunction of the sensorimotor area of the brain, which may suggest that clinical practice should improve sensorimotor disorders in ESRD patients from the perspective of adequate dialysis of uremic toxins.

Moreover, various machine classification models were used to capture the connectome gradient pattern information underlying ESRD. Most connectome gradient features with high discriminative power were mainly located in the PFC (dPFC, vPFC, vlPFC, and mpPFC) sensorimotor cortex, pCun/PCC, and insula. The PFC is a set of interconnected regions that have a unique but overlapping connectivity pattern with almost all sensory cortex and motor systems, as well as various subcortical structures^{41,42}. The dPFC and mpPFC are closely associated with cortical areas that emphasize information about motor and visuospatial processes, whereas the vlPFC is more heavily interconnected with cortical areas that emphasize stimulus identity and visual form information, and the vPFC is more associated with subcortical structures that process “internal” information such as homeostasis. The pCun/PCC is a highly connected and metabolically active brain region that internally supports directed cognition, episodic memory retrieval, visuospatial imagery, and self-processing operations^{43,44}. The insula has various functions, ranging from sensory processing to representing feelings, motor control, decision making, self-awareness, and complex social functions⁴⁵. Several previous studies have indicated disordered brain function and abnormal brain microstructure in ESRD patients, with abnormal regions mainly located in the PFC, sensorimotor cortex, cingulate cortex, and Ins^{15,35,46,47}. Our results indicated that these core connectome gradient dysfunctional regions served as neurological biomarkers of ESRD, emphasizing their importance for understanding the macroscale brain organization and hierarchical features underlying ESRD and its cognitive phenotype.

This study has several limitations. First, we did not evaluate sensorimotor symptoms in ESRD patients, such as uremic restless leg syndrome and uremic pruritus. Alternatively, we used the Neurosynth platform to investigate the association between ESRD-related functional gradient alterations and meta-analytic cognitive terms. Second, we didn't rule out the potential influence of drugs on cognition, such as erythropoietin⁴⁸, anti-hypertensive drugs⁴⁹, and Vitamin D⁵⁰, which are required for ESRD. Third, ESRD patients, who frequently have complaints of pain⁵¹ and fatigue⁵², were not assessed for the severity of these symptoms in the current study. These variables should be documented in future studies to evaluate their effects on cognition and functional gradients in ESRD. Fourth, the R-fMRI data acquisition included 185 functional volumes, which is slightly insufficient in quantity for data analysis. We also did not scan the field map to better correct the image distortions. Patients with chronic kidney diseases, especially those with ESRD, are unable to lie flat and remain still for a long time to complete the entire MRI scan. Therefore, on the basis of ensuring the quality of the T1-weighted structural images and R-fMRI images, we ultimately chose this protocol, which has been applied in our previous R-fMRI studies on ESRD patients^{10,11,16,35}. Subsequent research will optimize the scanning parameters to guarantee the quality of the R-fMRI. Finally, although sex and age differences did not reach statistical significance in the between-group comparisons, they approached marginal significance. Therefore, when comparing the differences in gradients and cognitive scale scores between-group, we incorporated age, sex, and education level as covariates in the regression analysis to control for potential confounding effects.

Materials and methods

Participants

This study was registered at ClinicalTrials.gov and approved by the local Research Ethics Review Board (NCT03191409, <https://clinicaltrials.gov/ct2/show/NCT03191409>) (Approval No. 2020G64). All experiments were

conducted under the Declaration of Helsinki, and all participants signed written informed consent. This study enrolled 77 right-handed ESRD patients (50 males, 27 females; mean age: 34 ± 10.05 years) undergoing maintenance hemodialysis between July 2020 and January 2023 (Fig. 1 and Table 1). All patients had a dialysis duration of >3 months. The exclusion criteria were ages <18 or >60 years, (2) psychiatric disorders or neurodegenerative disorders, (3) brain lesions (hemorrhage, head trauma, tumor, stroke, or encephalomalacia) based on conventional MRI or medical history, (4) smoking, alcohol, or drug abuse, (5) diabetic nephropathy, (6) visual or auditory disturbances (hearing loss, blurred vision, and other clinically relevant symptoms incompatible with a neuropsychological assessment), and (7) claustrophobia or other MR contraindications. The local community using advertisements recruited 48 right-handed, demographically matched HC (23 males, 25 females; mean age: 31 ± 8.16 years). The inclusion criteria for HC were age 18–60 years with no relevant medical history of neurologic, systemic, or psychiatric disease.

Clinical characteristics and neuropsychological assessment

Demographic characteristics and clinical data were collected from medical records. The underlying causes of ESRD included glomerulonephritis ($n = 58$), immunoglobulin A nephropathy ($n = 12$), and membranous nephropathy ($n = 7$). All ESRD patients had been receiving hemodialysis three times a week with a short midweek dialysis interval. The hemodialysis treatment lasted for ~4 h. with a mean kinetic transfer/volume urea (Kt/V) of >1.2⁵³. On the day before hemodialysis treatment, all patients underwent neuropsychological tests in a quiet room and blood tests. The neuropsychological tests included the AVLT-H, Montreal cognitive assessment (MoCA), and trail-making test (TMT), which were used to assess participant's global cognitive function, visuospatial skill, attention, orientation, language, conceptual thinking, executive function, and memory. Further, the Beck depression inventory (BDI) and Beck anxiety inventory (BAI) were administered to evaluate the mood disorder.

MR data acquisition and preprocessing

The MRI protocols included T1-fluid attenuated inversion recovery images (T1-FLAIR), T2-weighted periodically rotated overlapping parallel lines with enhanced reconstruction (T2-PROPELLER) images, individual high-resolution T1-weighted structural images, and R-fMRI scans for all participants. T1-FLAIR and T2-PROPELLER images were scanned to exclude intracranial lesions. All data for each participant were obtained using a Discovery MR750 3.0 T MR scanner equipped with an eight-channel phased-array head coil. Participants were instructed to lie quietly with their eyes closed and remain awake during the scan. Suitable foam padding and earplugs were used to reduce head motion and noise. The procedure was discontinued if any participant was uncomfortable or unable to complete the scan. After completing the scan, all participants were requested to verify their cooperation. The anatomical and functional data preprocessing were performed using fMRIPrep v23.1.4⁵⁴ and the eXtensible Connectivity Pipeline^{55,56}. All procedures were described in the supplementary materials.

Connectome gradient analysis

We used the open software BrainSpace (<https://github.com/MICA-MNI/BrainSpace>)²¹ to generate the connectome gradients for each participant. We first constructed a functional connectivity matrix for each individual by calculating Pearson's correlation coefficients of time series between each pair of brain regions defined using the Schaefer 7-network-based atlas with 400 parcels⁵⁷. The top 10% connections of each region were retained, representing the most typical connectivity profile of the connectome, and the resulting correlation coefficients were transformed by Fisher's r -to- z . The cosine similarity between each pair of regions based on the threshold connectivity profiles was calculated, taking advantage of the applicability of sparse vectors. We then applied diffusion map embedding^{19,58}, a nonlinear dimensionality reduction approach that is relatively robust to noise and computationally inexpensive, to capture the principal gradient components

that could explain connectome variance in descending order of the functional connectome. Diffusion map embedding transformed the relationships of the connectivity profiles into distances in the high-dimensional embedding space, ensuring a stable connectivity pattern representation, which created network regions with similar connectivity patterns spatially closer together in this space, whereas regions with only little or no interconnectivity are farther apart. Based on previous study recommendations^{19,58}, we set the manifold learning parameter of $\alpha = 0.5$ in the diffusion embedding process to retain the global relations. The resultant gradient maps were further analyzed to align across individuals using Procrustes rotation²⁷. We primarily focused on ESRD-related alterations in the first three components, which explained 38% of the variance. We then mapped back these components onto the cortical surface to visualize macroscale transitions in overall connectivity patterns at the system level²⁷.

For each gradient map, three global gradient metrics including the variance, range, and explanation ratios, were calculated. Specifically, the explanation ratio indicates the percentage of connectivity variance accounted for by a given gradient. A higher explanation ratio suggests that the embedding axis of this gradient captures a more dominant organizational pattern in the functional connectome. The gradient range measures the difference between the maximum positive and negative values across brain regions in a given gradient. A larger range indicates a greater differentiation in the encoded connectivity pattern between the regions localized at the gradient ends. The gradient variance represents the standard deviation of gradient scores across the brain. A higher value indicates stronger heterogeneity in regional connectivity architecture. A general linear model with age, sex, and education level as covariates was used to assess the between-group differences in functional connectome gradients. For the global gradient metrics, the statistical significance threshold was set to $P < 0.05$. For the surface-based gradient score maps, the statistical significance threshold was set to $P < 0.05$ after FDR correction.

Statistics and reproducibility

Association analysis of between-group gradient alterations, clinical characteristics, and neuropsychological variables. The between-group differences in demographics (age and educational level) and neuropsychological variables were compared using Kolmogorov–Smirnov, Levene’s, and independent two-sample *t*-tests (Kolmogorov–Smirnov test for normality, Levene’s test for determining the equality of variances, and Student’s *t*-test for equality of means) with Statistical Package for the Social Sciences (version 22.0, SPSS Statistics, IBM, Armonk, NY). A Chi-square test was used to test the between-group difference in gender ratio. Multiple linear regression analysis was utilized to correct the effect of age, sex, educational level, and mood disorder on the between-group differences in neuropsychological results. Pearson or Spearman correlation analysis was used to assess the relationships between gradient alterations and clinical characteristics and between gradient alterations and neuropsychological variables. The significance threshold was set to P values of < 0.05 after FDR correction.

Association analysis between ESRD-related gradient alterations and meta-analytic cognitive terms. We used Neurosynth³¹ (<https://neurosynth.org/>) to investigate the association between ESRD-related alterations of the first three connectome gradients and meta-analytic cognitive terms. First, we divided the between-group differences in each gradient into ESRD-positive (i.e., ESRD > controls) and ESRD-negative (i.e., ESRD < controls) maps. Second, we analyzed the resultant maps using the “decoder” function in Neurosynth to calculate the spatial correlation between these ESRD-positive and ESRD-negative maps and the meta-analytic map of each term in the Neurosynth database (version-7). We then selected the top 30 cognitive terms and further performed permutation tests (10,000 times) and FDR correction in which the spatial autocorrelations were corrected by generative modeling to estimate the significance of the correlation coefficients for each cognitive term.

Feature extraction and machine learning classification based on the ESRD-related gradient alterations. This study used seven commonly used classifiers in Python 3.11 (sklearn), including k-nearest neighbor, logistic regression, support vector machine, decision tree, random forest, gradient boosting decision tree, and XGBoost models, to determine whether between-group gradient alterations could discriminate ESRD patients from HCs. We used the LASSO method to select the most important features as a dimension reduction step to avoid overfitting and enhance model robustness. After performing LASSO, features with nonzero coefficients were retained to produce classification models. We then selected the 10-fold cross-validation strategy, which provides a good estimation of classifier generalizability^{59,60}. A permutation test, which randomly shuffles the label vectors of all participants 5000 times and then performs the same training and testing procedure described above for each permutation, was used to determine the significance of each classification model performance. After 5000 permutations, a null distribution for each model performance metric (accuracy, sensitivity, specificity, and AUC with 95% confidence intervals) was estimated. The P value of the significance of each metric was calculated by dividing the number of times higher than the actual value obtained by the nonpermutation model by the total number of permutations, and P values of < 0.05 were considered statistically significant. Finally, the resultant discriminative weight value for each feature was used to represent the feature contribution to the classification.

Validation analyses. Several validation analyses were conducted to verify the robustness of our results. First, in our main analyses, the BOLD data were preprocessed under the temporal filtering to 0.01–0.08 Hz. Meanwhile, we also set the temporal filtering range to 0.008–0.09 Hz for validation analyses. Second, we calculated and compared the mean FD between-group. Third, we use the LOOCV method as a supplementary validation approach.

Reporting summary

Further information on research design is available in the Nature Portfolio Reporting Summary linked to this article.

Data availability

The discovery data that support the findings are publicly available in the study’s Open Science Framework repository (<https://osf.io/f8eas/>).

Code availability

The main analysis codes are publicly available in the study’s Open Science Framework repository (<https://osf.io/f8eas/>). Diffusion embedding code is publicly accessible in the BrainSpace toolbox (<https://github.com/MICA-MNI/BrainSpace>).

Received: 14 October 2024; Accepted: 25 April 2025;

Published online: 06 May 2025

References

1. GBD Chronic Kidney Disease Collaboration Global, regional, and national burden of chronic kidney disease, 1990–2017: a systematic analysis for the Global Burden of Disease Study 2017. *Lancet* **395**, 709–733 (2020).
2. Viggiano, D. et al. Mechanisms of cognitive dysfunction in CKD. *Nat. Rev. Nephrol.* **16**, 452–469 (2020).
3. Scherer, J. S. et al. Sleep disorders, restless legs syndrome, and uremic pruritus: diagnosis and treatment of common symptoms in dialysis patients. *Am. J. Kidney Dis.* **69**, 117–128 (2017).
4. Flythe, J. E. et al. Symptom prioritization among adults receiving in-center hemodialysis: a mixed methods study. *Clin. J. Am. Soc. Nephrol.* **13**, 735–745 (2018).
5. Mettang, T. & Kremer, A. E. Uremic pruritus. *Kidney Int.* **87**, 685–691 (2015).

6. Ju, A. et al. Patient-reported outcome measures for fatigue in patients on hemodialysis: a systematic review. *Am. J. Kidney Dis.* **71**, 327–343 (2018).
7. Harris, T. J. et al. Pain, sleep disturbance and survival in hemodialysis patients. *Nephrol. Dial. Transpl.* **27**, 758–765 (2012).
8. Coluzzi, F. Assessing and treating chronic pain in patients with end-stage renal disease. *Drugs* **78**, 1459–1479 (2018).
9. O’Lone, E. et al. Cognition in people with end-stage kidney disease treated with hemodialysis: a systematic review and meta-analysis. *Am. J. Kidney Dis.* **67**, 925–935 (2016).
10. Li, P. et al. Neurovascular coupling dysfunction in end-stage renal disease patients related to cognitive impairment. *J. Cereb. Blood Flow. Metab.* **41**, 2593–2606 (2021).
11. Li, P. et al. Reversal of neurovascular decoupling and cognitive impairment in patients with end-stage renal disease during a hemodialysis session: Evidence from a comprehensive fMRI analysis. *Hum. Brain Mapp.* **44**, 989–1001 (2023).
12. Luo, S. et al. Abnormal intrinsic brain activity patterns in patients with end-stage renal disease undergoing peritoneal dialysis: a resting-state functional MR imaging study. *Radiology* **278**, 181–189 (2016).
13. Mu, J. et al. Altered white matter microstructure mediates the relationship between hemoglobin levels and cognitive control deficits in end-stage renal disease patients. *Hum. Brain Mapp.* **39**, 4766–4775 (2018).
14. Ni, L. et al. Aberrant default-mode functional connectivity in patients with end-stage renal disease: a resting-state functional MR imaging study. *Radiology* **271**, 543–552 (2014).
15. Ding, D. et al. The relationship between putamen-SMA functional connectivity and sensorimotor abnormality in ESRD patients. *Brain Imaging Behav.* **12**, 1346–1354 (2018).
16. Mu, J. et al. Abnormal interaction between cognitive control network and affective network in patients with end-stage renal disease. *Brain Imaging Behav.* **12**, 1099–1111 (2018).
17. Wang, Y. F. et al. The gut microbiota-inflammation-brain axis in end-stage renal disease: perspectives from default mode network. *Theranostics* **9**, 8171–8181 (2019).
18. Mesulam, M. M. From sensation to cognition. *Brain* **121**, 1013–1052 (1998).
19. Margulies, D. S. et al. Situating the default-mode network along a principal gradient of macroscale cortical organization. *Proc. Natl. Acad. Sci. USA* **113**, 12574–12579 (2016).
20. Krienen, F. M. & Sherwood, C. C. Gradients of connectivity in the cerebral cortex. *Trends Cogn. Sci.* **21**, 61–63 (2017).
21. Vos de Wael, R. et al. BrainSpace: a toolbox for the analysis of macroscale gradients in neuroimaging and connectomics datasets. *Commun. Biol.* **3**, 103 (2020).
22. Huntenburg, J. M., Bazin, P. L. & Margulies, D. S. Large-scale gradients in human cortical organization. *Trends Cogn. Sci.* **22**, 21–31 (2018).
23. Park, B. Y. et al. Differences in subcortico-cortical interactions identified from connectome and microcircuit models in autism. *Nat. Commun.* **12**, 2225 (2021).
24. Caciagli, L. et al. Disorganization of language and working memory systems in frontal versus temporal lobe epilepsy. *Brain* **146**, 935–953 (2023).
25. Xia, Y. et al. Development of functional connectome gradients during childhood and adolescence. *Sci. Bull.* **67**, 1049–1061 (2022).
26. Xia, M. et al. Connectome gradient dysfunction in major depression and its association with gene expression profiles and treatment outcomes. *Mol. Psychiatry* **27**, 1384–1393 (2022).
27. Hong, S. J. et al. Atypical functional connectome hierarchy in autism. *Nat. Commun.* **10**, 1022 (2019).
28. Tian, Y., Zalesky, A., Bousman, C., Everall, I. & Pantelis, C. Insula functional connectivity in schizophrenia: subregions, gradients, and symptoms. *Biol. Psychiatry Cogn. Neurosci. Neuroimaging* **4**, 399–408 (2019).
29. Dong, D. et al. Compressed sensorimotor-to-transmodal hierarchical organization in schizophrenia. *Psychol. Med.* **53**, 771–784 (2023).
30. Royer, J. et al. Cortical microstructural gradients capture memory network reorganization in temporal lobe epilepsy. *Brain* <https://doi.org/10.1093/brain/awad125> (2023).
31. Yarkoni, T. et al. Large-scale automated synthesis of human functional neuroimaging data. *Nat. Methods* **8**, 665–670 (2011).
32. Kiebel, S. J., Daunizeau, J. & Friston, K. J. A hierarchy of time-scales and the brain. *PLoS Comput. Biol.* **4**, e1000209 (2008).
33. Smallwood, J. et al. The default mode network in cognition: a topographical perspective. *Nat. Rev. Neurosci.* **22**, 503–513 (2021).
34. Buckner, R. L. & Krienen, F. M. The evolution of distributed association networks in the human brain. *Trends Cogn. Sci.* **17**, 648–665 (2013).
35. Li, P. et al. Altered intrinsic brain activity and memory performance improvement in patients with end-stage renal disease during a single dialysis session. *Brain Imaging Behav.* **12**, 1640–1649 (2018).
36. Giannaki, C. D. et al. Epidemiology, impact, and treatment options of restless legs syndrome in end-stage renal disease patients: an evidence-based review. *Kidney Int.* **85**, 1275–1282 (2014).
37. Koren, M. J. et al. Cognitive dysfunction and gait abnormalities in CKD. *Clin. J. Am. Soc. Nephrol.* **16**, 694–704 (2021).
38. Lin, Z. et al. Prevalence of restless legs syndrome in chronic kidney disease: a systematic review and meta-analysis of observational studies. *Ren. Fail.* **38**, 1335–1346 (2016).
39. Lu, P.-H. et al. Effects of uremic clearance granules in uremic pruritus: a meta-analysis. *Toxins* **13**, <https://doi.org/10.3390/toxins13100702> (2021).
40. De Deyn, P. P. et al. Endogenous guanidino compounds as uremic neurotoxins. *Kidney Int. Suppl.* **78**, S77–S83 (2001).
41. Miller, E. K. The prefrontal cortex and cognitive control. *Nat. Rev. Neurosci.* **1**, 59–65 (2000).
42. Miller, E. K. & Cohen, J. D. An integrative theory of prefrontal cortex function. *Annu. Rev. Neurosci.* **24**, 167–202 (2001).
43. Leech, R. & Sharp, D. J. The role of the posterior cingulate cortex in cognition and disease. *Brain* **137**, 12–32 (2014).
44. Cavanna, A. E. & Trimble, M. R. The precuneus: a review of its functional anatomy and behavioural correlates. *Brain* **129**, 564–583 (2006).
45. Gogolla, N. The insular cortex. *Curr. Biol.* **27**, R580–R586 (2017).
46. Mu, J. et al. White matter characteristics between amygdala and prefrontal cortex underlie depressive tendency in end stage renal disease patients before the dialysis initiation. *Brain Imaging Behav.* **15**, 1815–1827 (2021).
47. Song, S. H. et al. Cerebral glucose metabolism abnormalities in patients with major depressive symptoms in pre-dialytic chronic kidney disease: statistical parametric mapping analysis of F-18-FDG PET, a preliminary study. *Psychiatry Clin. Neurosci.* **62**, 554–561 (2008).
48. Lee, S. T. et al. Erythropoietin improves memory function with reducing endothelial dysfunction and amyloid-beta burden in Alzheimer’s disease models. *J. Neurochem.* **120**, 115–124 (2012).
49. Birkenhager, W. H. & Staessen, J. A. Antihypertensives for prevention of Alzheimer’s disease. *Lancet Neurol.* **5**, 466–468 (2006).
50. Latimer, C. S. et al. Vitamin D prevents cognitive decline and enhances hippocampal synaptic function in aging rats. *Proc. Natl. Acad. Sci. USA* **111**, E4359–E4366 (2014).
51. Brkovic, T., Burilovic, E. & Puljak, L. Risk factors associated with pain on chronic intermittent hemodialysis: a systematic review. *Pain. Pract.* **18**, 247–268 (2018).
52. Bossola, M. & Tazza, L. Postdialysis fatigue: a frequent and debilitating symptom. *Semin. Dial.* **29**, 222–227 (2016).
53. Daugirdas, J. T. Kt/V (and especially its modifications) remains a useful measure of hemodialysis dose. *Kidney Int.* **88**, 466–473 (2015).
54. Esteban, O. et al. fMRIPrep: a robust preprocessing pipeline for functional MRI. *Nat. Methods* **16**, 111–116 (2019).

55. Ciric, R. et al. Mitigating head motion artifact in functional connectivity MRI. *Nat. Protoc.* **13**, 2801–2826 (2018).
56. Satterthwaite, T. D. et al. An improved framework for confound regression and filtering for control of motion artifact in the preprocessing of resting-state functional connectivity data. *Neuroimage* **64**, 240–256 (2013).
57. Schaefer, A. et al. Local-global parcellation of the human cerebral cortex from intrinsic functional connectivity MRI. *Cereb. Cortex* **28**, 3095–3114 (2018).
58. Coifman, R. R. et al. Geometric diffusions as a tool for harmonic analysis and structure definition of data: diffusion maps. *Proc. Natl. Acad. Sci. USA* **102**, 7426–7431 (2005).
59. Varoquaux, G. et al. Assessing and tuning brain decoders: cross-validation, caveats, and guidelines. *Neuroimage* **145**, 166–179 (2017).
60. Varoquaux, G. Cross-validation failure: small sample sizes lead to large error bars. *Neuroimage* **180**, 68–77 (2018).

Acknowledgements

The authors wish to thank all the patients with ESRD who participated in this study. We owe our gratitude to the clinical team of the department of Nephropathy in Nuclear Industry 215 Hospital. This study was funded by the National Natural Science Foundation of China (Grant No. 82071879, 82202121), the Health Research and Innovation Capacity Strengthening Platform Program of Shaanxi Province (Grant No.2023PT-09), the Hovering Program of Fourth Military Medical University (axjhw), the Talent Foundation of Tangdu Hospital (2018BJ003), the Key Research and Development Plan of Xianyang City (Grant No. L2023-ZDYF-SF-035 and L2022ZDYF-SF-026), the Natural Science Major Basis Research Project in Shaanxi Province (No. 2017ZDJC-13), the Science and Technology Research Project of Shaanxi Nuclear Industry Group Co., Ltd (Grant No. 61240302), the Natural Science Basis Research Plan in Shaanxi Province (No. 2023-JC-QN-0984), the Clinical Research Award of the First Affiliated Hospital of Xi'an Jiaotong University (No. XJTU1AF-CRF-2023-021).

Author contributions

M.Z., W.W., and J.Y.M. drafted the work and revised it critically for important intellectual content. P.L. and N.L. made substantial contributions to the conception or design of the work; or the acquisition, analysis, or interpretation of data for the work. L.R., Y.P.Y., X.Y.Z., H.J.Y., and Z.Y.L. revised the article and interpreted the data. All authors approved the version submitted for publication.

Competing interests

The authors declare no competing interests.

Additional information

Supplementary information The online version contains supplementary material available at <https://doi.org/10.1038/s42003-025-08132-6>.

Correspondence and requests for materials should be addressed to Jun-Ya Mu, Wen Wang or Ming Zhang.

Peer review information *Communications Biology* thanks Pedro Henrique Rodrigues da Silva, Clare Kelly, and the other, anonymous, reviewer(s) for their contribution to the peer review of this work. Primary Handling Editor: Christina Karlsson Rosenthal.

Reprints and permissions information is available at <http://www.nature.com/reprints>

Publisher's note Springer Nature remains neutral with regard to jurisdictional claims in published maps and institutional affiliations.

Open Access This article is licensed under a Creative Commons Attribution-NonCommercial-NoDerivatives 4.0 International License, which permits any non-commercial use, sharing, distribution and reproduction in any medium or format, as long as you give appropriate credit to the original author(s) and the source, provide a link to the Creative Commons licence, and indicate if you modified the licensed material. You do not have permission under this licence to share adapted material derived from this article or parts of it. The images or other third party material in this article are included in the article's Creative Commons licence, unless indicated otherwise in a credit line to the material. If material is not included in the article's Creative Commons licence and your intended use is not permitted by statutory regulation or exceeds the permitted use, you will need to obtain permission directly from the copyright holder. To view a copy of this licence, visit <http://creativecommons.org/licenses/by-nc-nd/4.0/>.

© The Author(s) 2025